
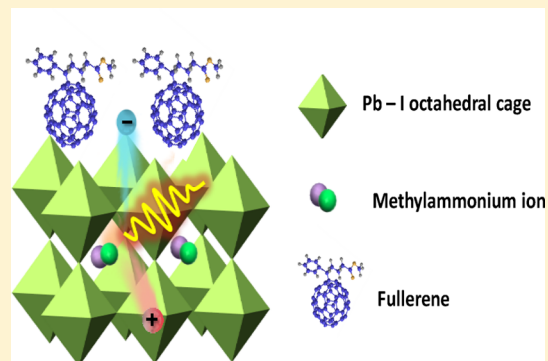


# The Functions of Fullerenes in Hybrid Perovskite Solar Cells

YanJun Fang, Cheng Bi, Dong Wang, and Jinsong Huang\*

Department of Mechanical and Materials Engineering, University of Nebraska—Lincoln, Lincoln, Nebraska 68588-0656, United States

**ABSTRACT:** There is increasing interest in the application of fullerene-based carbon materials in perovskite solar cells for increased efficiency, reduced hysteresis, and improved stability. This Perspective summarizes the progress in the understanding of the function of fullerenes in perovskite solar cells in blocking leakage through pin-holes, passivating the defects at the perovskite film surfaces and grain boundaries, and modulating the open-circuit voltage of the devices. We also critically reviewed several open questions on the functions of fullerenes in perovskite solar cells based mainly on recent progress: How do fullerenes reduce current hysteresis? What is the function of double-fullerene layers? Does the doping of the fullerene by perovskite contribute to eliminating the photocurrent hysteresis at room temperature? Why do some perovskite/fullerene solar cells still have hysteresis at low temperature? Are perovskite solar cells with fullerenes in the intergranular boundaries bulk heterojunction solar cells? Finally, the impact of the fullerene on perovskite solar cell stability is discussed.



Organic–inorganic halide perovskite materials are among the most promising candidates for next-generation low-cost and highly efficient solar cells benefiting from their excellent optoelectronic properties including high absorption coefficient, high carrier mobility, and long carrier diffusion length.<sup>1–6</sup> The power conversion efficiency (PCE) of perovskite solar cells (PSCs) has increased to over 20% in the past few years with improved perovskite film quality as well as better charge transport layers.<sup>7–13</sup> Carbon materials have been intensively applied in perovskite solar cells for multiple purposes. Amorphous carbon was shown by Mei et al. to work as electrode and encapsulation layer.<sup>14</sup> Carbon nanotubes, including single-walled and multiple-walled ones, were shown to be effective hole transport materials for perovskites,<sup>15–18</sup> which efficiently extracted holes and formed long-living charge-separated states with electrons in perovskite.<sup>19</sup> Graphene, as a typical form of two-dimensional carbon material, was first shown by Wang et al. to work as an efficient electron extraction layer for perovskites when mixing with low-temperature hydrothermal grown TiO<sub>2</sub> nanoparticles.<sup>20</sup> Benefiting from its high transparency, high conductivity, and excellent mechanical flexibility, graphene was successfully used as transparent electrode in perovskite-based flexible solar cells, which exhibited superb stability against bending deformation, maintaining 85% of their initial PCE after 5000 bending cycles.<sup>21</sup> Recently, Hadadian et al. also demonstrated the morphology tuning and interfacial passivation effects of nitrogen-doped reduced graphene oxide on the perovskite layer

when blending them together, which resulted in a much improved open-circuit voltage to 1.15 V.<sup>22</sup>

Fullerene and its derivatives have been widely used in organic solar cells as acceptors during the past decades. Fullerenes as electron acceptors for perovskites were initially demonstrated in the study of carrier diffusion length in perovskite where a clear quenching of perovskite photoluminescence by phenyl-C61-butyric acid methyl ester (PCBM) was observed.<sup>1,2</sup> Fullerenes were first introduced into perovskite solar cells by Jeng et al. to form fullerene/perovskite planar heterojunction (PHJ) solar cells with a highest reported efficiency of ~3.9% (Figure 1a),<sup>23</sup> and the efficiency was soon increased to 7.4% by Sun et al. in 2014.<sup>24</sup> However, the large amount of pin-holes in the noncontinuous perovskite films fabricated by spin-coating the directly mixed lead iodide (PbI<sub>2</sub>) and methylammonium halide (MAI) blend precursor solution limited the performance of the devices. By tuning the precursor ratio of PbI<sub>2</sub>/MAI to 0.7–0.8 in a single-step spin-coating deposition of CH<sub>3</sub>NH<sub>3</sub>PbI<sub>3</sub> (MAPbI<sub>3</sub>), we were able to improve the quality of the films, because the additional MAI can slow the nucleation and growth of the grains. The efficiency of perovskite/fullerene solar cells was increased to over 12% with a fill factor exceeding 80% demonstrated for the first time for perovskite solar cells.<sup>25</sup> By improving the perovskite film coverage with a two-step interdiffusion method and by increasing the grain sizes with

Received: December 4, 2016

Accepted: March 3, 2017

Published: March 3, 2017

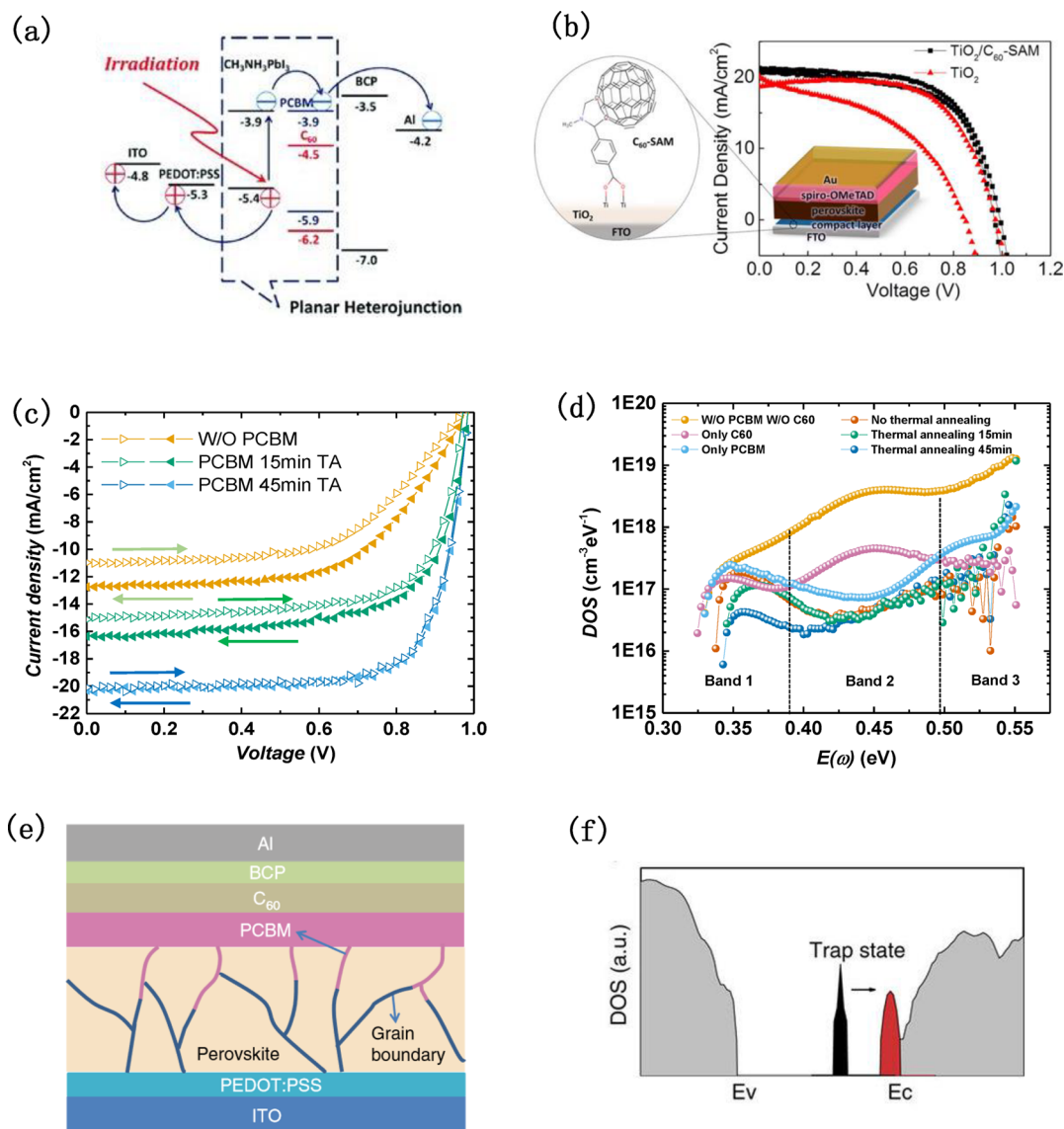
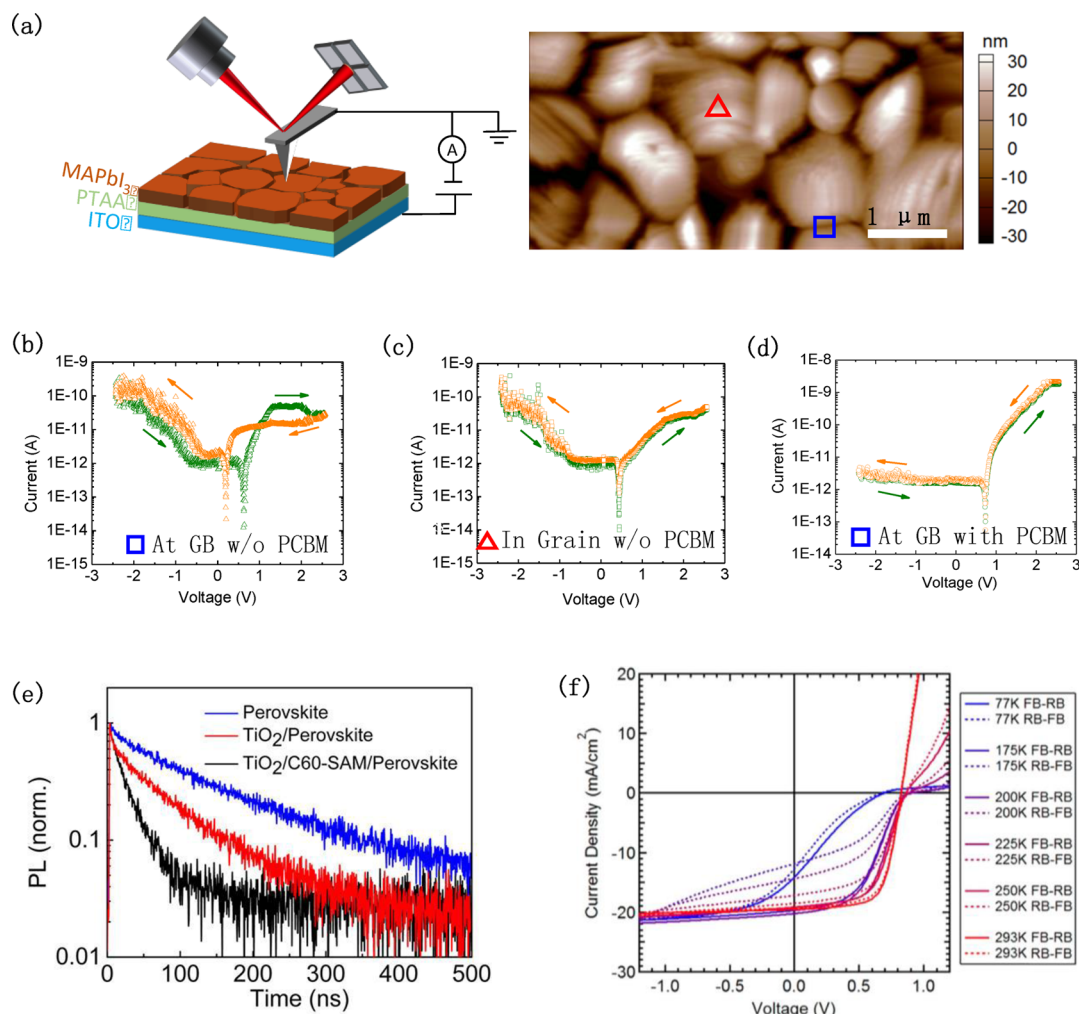


Figure 1. (a) Scheme of the energy levels of the planar heterojunction perovskite solar cells. (Reprinted with permission from ref 23. Copyright 2013 Wiley.) (b) Current–voltage curves of perovskite solar cells with C<sub>60</sub>-SAM-modified (red) and unmodified TiO<sub>2</sub> compact layer (black). (Reprinted from ref 36. Copyright 2014 American Chemical Society.) (c) Photocurrents for devices without a PCBM layer (orange) and with PCBM layers thermally annealed for 15 min (green) and 45 min (blue). (d) tDOS of perovskite solar cells before and after fullerene passivation. (e) Schematic of the diffusion of fullerene into the grain boundaries thus passivating the trap states there. (Reprinted with permission from ref 30. Copyright 2014 Nature Publishing Group.) (f) Schematic of calculated tDOS by DFT in perovskite before (black) and after (red) PCBM passivation. (Reprinted with permission from ref 31. Copyright 2015 Nature Publishing Group.)

hydrophobic substrate surface and abnormal grain growth mode, we quickly increased the device efficiency to over 18%.<sup>26–28</sup> We further reduced the energy disorder by solvent annealing of fullerenes and charge recombination at the perovskite/fullerene interfaces with tunneling junction, which further boosted the PCE to over 20% with the photoactive layer of MAPbI<sub>3</sub>.<sup>12,29</sup>

It was soon realized by us that fullerene layers not only functioned as an electron transport layer (ETL) but also played an important role in passivating the charge traps at the surfaces and grain boundaries of perovskite thin films, which significantly suppressed the notorious current–voltage hysteresis and increased the PCE of the perovskite solar cells.<sup>30</sup> We speculated that fullerene could diffuse along the grain boundaries to passivate the defects at grain boundaries, while the difference of the photoluminescence spectra from the

perovskite bottom surface and fullerene covered top surface indicates that fullerene could not completely diffuse through the whole films under the optimized thermal annealing conditions for most efficient solar cells. To address this issue, Xu et al.<sup>31</sup> and Chiang et al.<sup>32</sup> mixed the fullerenes in perovskite precursors to intentionally drive fullerenes into the grain boundaries during the perovskite film formation, and very high fill factor above 80% has been achieved in this kind of device.<sup>32,33</sup> In addition, Han and colleagues proposed a graded-heterojunction structure in which PCBM was incorporated into the top surface of the perovskite layer with a gradient distribution.<sup>34</sup> While the intercalation of PCBM in perovskite crystal structure is not possible because of the too large PCBM molecules, the PCBM molecules most likely stay at the top surface as well as grain boundaries of perovskite in the top layer, as proposed in our initial study.<sup>30</sup> Nevertheless, the



**Figure 2.** (a) Schematic of conductive AFM measurement setup and the corresponding topography AFM image of the perovskite thin film. (b–d) Local current–voltage hysteresis measured by conductive AFM (b) at grain boundary, (c) in grain interior, and (d) at grain boundary after coating with PCBM. (Reprinted with permission from ref 41. Copyright 2016 Royal Society of Chemistry.) (e) Photoluminescence decays of bare perovskite film (black), perovskite film on top of  $\text{TiO}_2$  (red), and perovskite film on top of  $\text{C}_{60}$ -SAM modified  $\text{TiO}_2$  (blue). (Reprinted from ref 36. Copyright 2014 American Chemical Society.) (f) Current–voltage curves for a fullerene top cathode  $\text{MAPbI}_3$  solar cell in a sweep direction from forward to reverse bias (solid line) and reverse to forward bias (dashed line) at temperatures ranging between 77 and 293 K. (Reprinted from ref 46. Copyright 2015 American Chemical Society.)

compact and conformal coating of PCBM with thickness of 50 nm effectively suppressed the dark current, which resulted in a high PCE > 18% in centimeter-scale perovskite solar cells. In addition, fullerenes are becoming more popular as an interfacial modification layer between oxides ETL, including  $\text{TiO}_2$  and  $\text{SnO}_2$ , and perovskite to promote the electron transfer from perovskite to  $\text{TiO}_2$  or  $\text{SnO}_2$  as well as to passivate the interfacial trap states, which generally results in much smaller current–voltage hysteresis and higher PCE (Figure 1b).<sup>35–39</sup>

Despite the quick progress in the application of fullerenes in perovskite solar cells during the past few years, there are still some important open questions regarding the function of fullerene in perovskite solar cells, such as how exactly fullerenes reduce the current hysteresis, what is the impact of fullerenes on the open-circuit voltage ( $V_{\text{OC}}$ ) and device stability of perovskite solar cells, and whether the perovskite/fullerene hybrid solar cell is a bulk heterojunction (BHJ) cell. In the following sections, we comment on these questions based on our recent progress, aiming to deepen the fundamental understanding of the actual role(s) played by fullerenes.

**Function of Fullerenes on Current Hysteresis.** Current–voltage hysteresis, i.e., the scan direction-dependent nonoverlapping current–voltage curves, has been widely observed in non-optimized perovskite solar cells.<sup>40</sup> We reported the first hysteresis-free perovskite solar cells by using fullerenes as ETL (Figure 1c).<sup>25</sup> The perovskite solar cells with fullerenes usually exhibited less or no hysteresis in comparison to those with  $\text{TiO}_2$  as ETL. After a couple of years’ studies worldwide, the consensus slowly developed that the origins of current hysteresis are charge traps, ion migration, or interfacial charge accumulation.<sup>30,41</sup> Therefore, the fullerenes have to overcome all these possible channels that all cause current hysteresis. First, we proposed for the first time that fullerenes could effectively passivate the trap states at the surfaces and grain boundaries of the polycrystalline perovskite layer, which was confirmed by the direct trap density measurement of the perovskite film with and without fullerene coating by thermal admittance spectroscopy (TAS).<sup>30</sup> As shown in Figure 1d, the total trap density of states (tDOS) at the higher-energy region (>0.4 eV), which were most likely from the top surface of the

perovskite layers, were decreased by nearly 2 orders of magnitude right after the deposition of PCBM/ $C_{60}$  double-fullerene layer; the shallower trap states ( $<0.4$  eV) that mainly originated from grain boundaries could be passivated only by driving PCBM into the grain boundaries during the thermal annealing process (Figure 1e). There has not been much theoretical study on why fullerenes can passivate the charge traps on perovskite surface. Sargent and colleagues discovered the formation of PCBM-halide radical after mixing PCBM and perovskite precursor solution and revealed based on density functional theory (DFT) that it is thermodynamically favored for the bonding of PCBM with Pb–I antisite defect which suppressed the formation of deep trap states (Figure 1f).<sup>31</sup> More theoretical work is needed to understand the passivation mechanism, which is, however, limited by the understanding of surface and grain boundary defects on perovskite films. Second, fullerene may block the ion migration along the grain boundaries, the dominating ion migration channel in polycrystalline perovskite thin films, as confirmed by us with local current–voltage measurements (Figure 2a).<sup>41</sup> As shown in Figure 2b–d, the current–voltage hysteresis measured by conductive atomic-force microscopy (AFM) was much more significant at the grain boundary region in comparison to the grain interior for the perovskite film without the coating of PCBM, while the film covered by PCBM layer showed negligible hysteresis even at the grain boundary. This indicates that the ion diffusion is suppressed because of the filling of the relatively open grain boundaries with the nonmobile, big-sized fullerenes.<sup>31</sup> Third, the charge accumulation issue is negligible at the perovskite/fullerene interface in comparison to the  $TiO_2$ /perovskite interface. This is because the charge-transfer rate between fullerene and perovskite is much faster than that between perovskite and  $TiO_2$ , which is evidenced by the increased photoluminescence decay rate when the perovskite and  $TiO_2$  interface is modified by fullerene (Figure 2e).<sup>36,37</sup> We recently showed the charge extraction in perovskite/fullerene PHJ solar cells can be shorter than 1 ns,<sup>42</sup> which again indicates the negligible charge accumulation at the perovskite/fullerene interface.

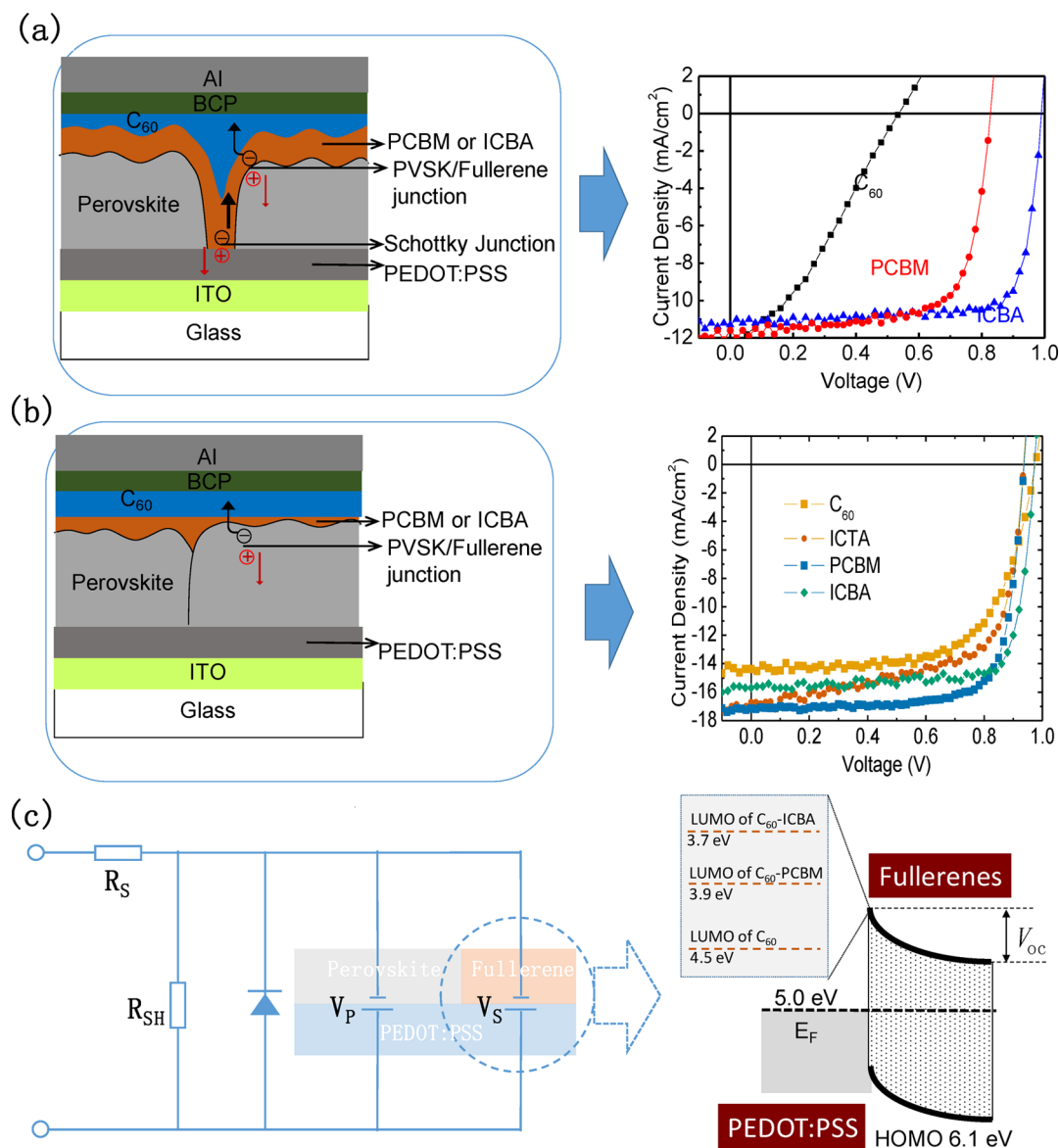
**Perovskite solar cells with fullerene interfacial layers generally have much less or no current hysteresis in devices with both planar and mesoporous heterojunction structures.**

It is worth noting that the combination of PCBM and  $C_{60}$  double-fullerene layers is found by us to be always necessary to achieve the highest efficiency, in addition to eliminating the current hysteresis. The spun fullerenes (either  $C_{60}$  or other derivatives) form the conformal covering layer on the perovskite film surfaces to fill possible pin-holes, while the thermal evaporated fullerene can further cover the pin-holes in the first fullerene layer, which effectively eliminates the leakage current. In addition, PCBM and  $C_{60}$  were shown to have different but complementary trap passivation capabilities.<sup>25</sup> According to the TAS measurement results shown in Figure 1d, PCBM tends to passivate the trap states in bands 1 and 2, while  $C_{60}$  prefers to passivate trap states in bands 1 and 3. The devices with PCBM/ $C_{60}$  double-fullerene layer show a trap passivation effect that is better than that of devices with only

one type of fullerene layer. The excellent trap passivation effect of double-fullerene layer was further demonstrated by us with the elimination of flicker noise in perovskite photodetectors. Flicker noise can be induced by carrier density fluctuation due to the trapping and detrapping of charge carriers during their transportation, and the absence of flicker noise is a strong indication of low density of deep traps.<sup>43</sup>

The discovery of enhanced conductivity of PCBM by blending with precursor MAI<sup>44</sup> raised the question whether it is the dominating mechanism in eliminating the current hysteresis by efficiently collecting charge. In fact, the doping of fullerenes by iodine-containing molecules has been previously developed for highly conductive fullerene materials.<sup>45</sup> Bai et al. actually took advantage of this doping effect to enhance the conductivity of a low-mobility fullerene derivative to reduce the contact resistance and enhance the device fill factors.<sup>44</sup> However, its contribution to hysteresis reduction might not be significant for the following reasons. First, an increased series resistance in any type of solar cells will change only the device efficiency but should not cause a hysteresis. It was confirmed by Bai et al. that the device without a doped fullerene layer did not show hysteresis either. Second, one would argue that if the low conductivity of the charge transport layers is the origin of current hysteresis, it would already be easily eliminated by using much more conductive metal electrodes, which is not the case. Third, the doping-induced conductivity enhancement of fullerenes usually increases carrier concentration, while the charge extraction relies more on the mobility of the fullerene layer. Finally, one may also argue the dynamic doping and dedoping of fullerene induced by ion diffusion could cause a dynamic variation of the series resistance in the fullerene layer, which may cause the hysteresis. A simple calculation of the fullerene conductivity shows that it will not induce notable resistivity and voltage loss during the current scanning, once its thickness is small enough ( $<20$  nm). In addition, removing fullerene should have eliminated this hysteresis origin, which is however opposite to the experimental observations. By the same token, the doping of poly(3,4-ethylenedioxythiophene) polystyrenesulfonate (PEDOT:PSS) by the perovskite should not play a major role in reducing hysteresis in perovskite solar cells, because hole transport layers (HTL) with much lower conductivity, such as poly[bis(4-phenyl)(2,4,6-trimethylphenyl)amine (PTAA), will not cause hysteresis either. As long as the PTAA layer thickness is small enough, its conductivity does not limit the efficiency of perovskite solar cells either, even without any doping.

Recently, Durrant and colleagues discovered an interesting phenomenon that the perovskite solar cells with PCBM as cathode exhibited apparent hysteresis at low temperature, even if they were hysteresis-free at room temperature (Figure 2f).<sup>46</sup> The ion-migration issue could be ruled out as the origin of the hysteresis at low temperature, because the ion migration should be frozen at low temperature. We speculate that one possible reason to explain this phenomenon is that fullerenes might be more effective in passivating the deep traps on the perovskite film surface, whereas the unpassivated shallow traps, which do not affect the carrier transport at room temperature because of thermal activation, could behave as “deep traps” at low temperature. These shallower traps can be still too deep for the trapped carriers to escape, because the thermal activation energy,  $k_B T$ , is much smaller at lower temperature. Therefore, the consequent slow trapping and detrapping events would cause the hysteresis. In this context, we can estimate the



**Figure 3.** Schematic device structure of the perovskite solar cell devices (a) with and (b) without pin-holes and the corresponding photocurrent curves with different fullerene layers. (Adapted with permission from ref 25. Copyright 2014 Royal Society of Chemistry. Reprinted with permission from ref 50. Copyright 2015 Wiley.) (c) Schematic diagram of the perovskite solar cell and Schottky cell connected in parallel.

“shallower-traps” have an energy depth in the range of tens of millielectronvolts. In many cases, the measured exciton binding energies derived from temperature-dependent photoluminescence and absorption spectra are in this range,<sup>47–49</sup> which indicates they may have the same origin of energy disorder, and the excitons are dominantly bound excitons, rather than free excitons.

**Function of Fullerenes in  $V_{OC}$  of Perovskite Solar Cells.** A fullerene-type-dependent  $V_{OC}$ , i.e., fullerenes with high lowest unoccupied molecular orbital (LUMO) typically resulted in higher  $V_{OC}$ , was observed in the early studies<sup>23,25</sup> (Figure 3a), which is difficult to explain using thin-film solar cell theory. In parallel, studies conclusively show that free carriers, instead of bound Frenkel excitons, are generated in the hybrid perovskites.<sup>48</sup> This was interpreted by us as a second Schottky junction formation between fullerene and the hole transport material PEDOT:PSS in a device with structure of ITO/PEDOT:PSS/perovskite/fullerene/Al, in addition to the per-

ovskite/fullerene junction, because the perovskite films still had many pinholes (Figure 3c). The PEDOT:PSS/fullerene junction is sensitive to the LUMO of fullerenes, and a lower  $V_{OC}$  from PEDOT:PSS/fullerene junction could drag down the total device  $V_{OC}$ . This interpretation was confirmed once we were able to form compact, pinhole-free perovskite films with a two-step solution-processed interdiffusion method where the double  $PbI_2$  and MAI layers were spun from orthogonal solvents.<sup>26</sup> The  $V_{OC}$  of the perovskite/fullerene solar cells were independent of fullerene type once fullerenes cannot contact the HTL directly (Figure 3b).<sup>50</sup> It was also confirmed by many other follow-up studies using very thick PCBM layer<sup>51,52</sup> to block the leakage pin-holes or using the thermal evaporation method.<sup>53</sup> For the mixed perovskite:PCBM solar cells, the  $V_{OC}$  is usually smaller than that of the fullerene-based PHJ devices with pinhole-free perovskite film.<sup>32,33</sup> This can again be explained by the formation of a Schottky junction between PCBM with the HTL. Because PCBM is premixed in the

precursor, there will be inevitably direct contact between PCBM and PEDOT:PSS, which has a Schottky junction barrier height of 0.8 eV.

The open-circuit voltage of perovskite solar cells with fullerenes is correlated to the quasi Fermi level of the fullerene layers, which are determined by the energy disorder of fullerenes.

After a brief literature survey, it was puzzling for us to find that fullerene-based planar heterojunction perovskite solar cells usually exhibited a  $V_{OC}$  lower than that of the  $TiO_2$ -based mesoporous-structure devices. In order to enhance the device  $V_{OC}$  of perovskite solar cells with fullerene as ETL, we paid attention to the energy disorder of fullerenes.<sup>29</sup> When the perovskite film was pinhole-free, there would be no Schottky junction formed between the fullerene and PEDOT:PSS, and the  $V_{OC}$  should in principle be determined by the quasi Fermi level splitting in the devices, which was affected by not only the perovskite layer but also by the charge transport layer. Because of the high crystallinity of the perovskite materials and many other reasons, the conduction band and valence band edges are very sharp. On the other hand, the amorphous fullerene layer is usually subject to a wide distribution of band tail states originating from their structural, chemical, and dynamical disorder. As illustrated in Figure 4a, these tail states in fullerene layers will reduce the quasi Fermi level splitting. Therefore, the  $V_{OC}$  of perovskite solar cells were essentially determined by the energy disorder in the fullerene layer, rather than the LUMO of fullerenes.<sup>29</sup> It is worth emphasizing that these energy disorder-induced electronic states are not charge trap states, because the charge carriers transferred to these states can still be extracted to the cathode without causing hysteresis. Therefore, the short-circuit current and fill factor are not affected by energy disorder of fullerenes. The existence of energy disorder can explain why the devices with 1',1'',4',4''-tetrahydro-di[1,4]methano-naphthaleno[1,2:2',3',5,6:60:2'',3''] [5,6]fullerene  $C_{60}$  (ICBA) or indene  $C_{60}$  trisadduct (ICTA) as ETL still show considerable

efficiency, even though the LUMO of ICBA or ICTA is higher than the conduction band of  $MAPbI_3$ .<sup>50</sup> The energy disorder of amorphous PCBM is contributed by both the static origin of loose packing and the dynamic origin of vibration interactions.<sup>54</sup> To suppress the static disorder, we applied a simple solvent annealing method to enhance the PCBM structural ordering, and the measured energy disorder parameter  $\sigma_n$ , which represents the broadening of the density of states, decreased from 136 to 90 meV (Figure 4b).<sup>29</sup> The measured energy disorder parameter variation was in excellent agreement with an independent theoretical work by Brédas and co-workers.<sup>54</sup> The  $V_{OC}$  was increased by 50 mV on average to 1.13 V for the solvent-annealed devices without sacrificing short-circuit current or fill factor. The comparable  $V_{OC}$  of the device with fullerene and  $TiO_2$  also indicates that the energy disorder in high-temperature annealed polycrystalline  $TiO_2$  is also quite small, which is still a puzzle to us.

To further increase the  $V_{OC}$  of fullerene-based perovskite solar cells, one possible strategy is to dope the fullerene layer. The doping itself will hardly reduce the energy disorder of the fullerene layer, but the increased carrier concentration may fill the low-energy states and shift the Fermi level of the fullerene layer upward to align better with the quasi Fermi level of electrons in the perovskite under illumination. In fact, a similar strategy was applied on  $SnO_2$  ETL to enhance  $V_{OC}$ . N-type doping of the inorganic ETL  $SnO_2$  by Sb increased the  $V_{OC}$  by 60 mV, which is in agreement with the Fermi level shift of the  $SnO_2$  as a result of carrier concentration increase.<sup>55</sup> However, the doping concentration should not be too high, otherwise it would cause additional interfacial recombination between electrons in PCBM and holes in perovskite, which would reduce the quasi Fermi level splitting and consequently the  $V_{OC}$ .

*Is Perovskite:PCBM Blend a Bulk Heterojunction?* Very high fill factors of 80%–82% have been achieved recently in PHJ perovskite solar cells with fullerene intentionally incorporated in precursor solution so that fullerenes can be incorporated at the grain boundaries. One proposed scenario was that the fullerene intergranular layers act as electron transport channel, making the perovskite solar cells resemble BHJ-based organic

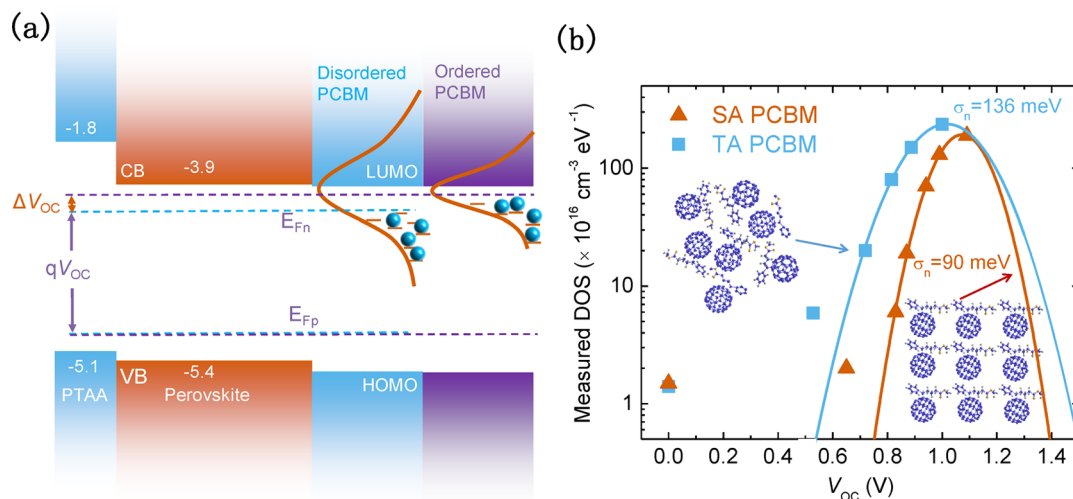


Figure 4. (a) Schematic illustration of how energy disorder of the PCBM layer influences the device  $V_{OC}$ . (b) Measured DOS of devices with solvent annealed PCBM (red) and thermal annealed PCBM (blue). (Adapted with permission from ref 29. Copyright 2016 Nature Publishing Group.)

solar cells.<sup>32,33</sup> The BHJ structure is required in efficient organic solar cells, because the exciton diffusion length in organic semiconductor materials is much less than the optical absorption length. Fullerenes are introduced to form BHJ with other p-type polymers to facilitate exciton separation and electron transportation.

The mobility of perovskites is several orders of magnitude larger than that of fullerenes, making perovskites the preferred channel for electron extraction.

There is still no direct evidence for the formation of fullerene percolation network along the grain boundaries, which will need further study from morphology characterization. On the other hand, even if the fullerene intergranular layers formed a percolation network, it is questionable whether electrons will go through the fullerene intergranular layer in perovskite solar cells. Perovskite materials have reported hole and electron mobility in the range of 6–200 cm<sup>2</sup>/(V s) depending on the chemical composition and crystallinity, which are remarkably high for solution-processed semiconductors, while fullerenes generally have 3–5 orders of magnitude lower mobility [10<sup>-4</sup>–10<sup>-3</sup> cm<sup>2</sup>/(V s)]. It is difficult for electrons to choose the much lower mobility channels. Herein, we use a simple design of light-emitting diode (LED) to demonstrate the much better charge mobility in perovskite materials and much faster drift of carrier through the perovskite layer compared to that of organic charge transport layers. As illustrated in Figure 5, we fabricated

LED devices with a structure of ITO/PTAA/MAPbCl<sub>x</sub>Br<sub>3-x</sub>/bathophenanthroline (Bphen)/Al. The PTAA layer served as hole injection layer as well as electron-blocking layer, while the Bphen served as electron injection and hole-blocking layer. The design was intended to make a perovskite LED by confining electrons and holes in the perovskite layer for radiative recombination. However, the device showed sky blue electroluminescence with a peak at 500 nm, which actually came from the emission of the PTAA layer. This result can be explained by the fact that the electron transport time through the perovskite layer is much shorter than hole transport time through the PTAA layer. Thus, the electrons go through the perovskite layer and recombined with the holes within the PTAA layer. Considering the hole mobility in PTAA measured by space-charge-limited current method is 10<sup>-3</sup>–10<sup>-2</sup> cm<sup>2</sup>/(V s), which is comparable or slightly greater than the electron mobility in regular fullerene materials, the solution-processed perovskite thin films should possess an electron mobility much larger than this value.

Recent ultrafast photodetector study with transient photocurrent (TPC) measurement reveals the very fast electron extraction in the regular perovskite solar cells. With a regular solar cell structure of ITO/PTAA/MAPbI<sub>3</sub>/C<sub>60</sub>/bathocuproine (BCP)/Cu (device type I), Shen et al. showed that photo-generated electrons could be extracted out of the solar cells by the built-in electric field at short-circuit conditions in the subnanosecond range after generation (Figure 6 b).<sup>42</sup> A time-resolved photoluminescence system was actually constructed with the perovskite photodetectors. We also followed the method reported by Chiang et al. to intentionally incorporate

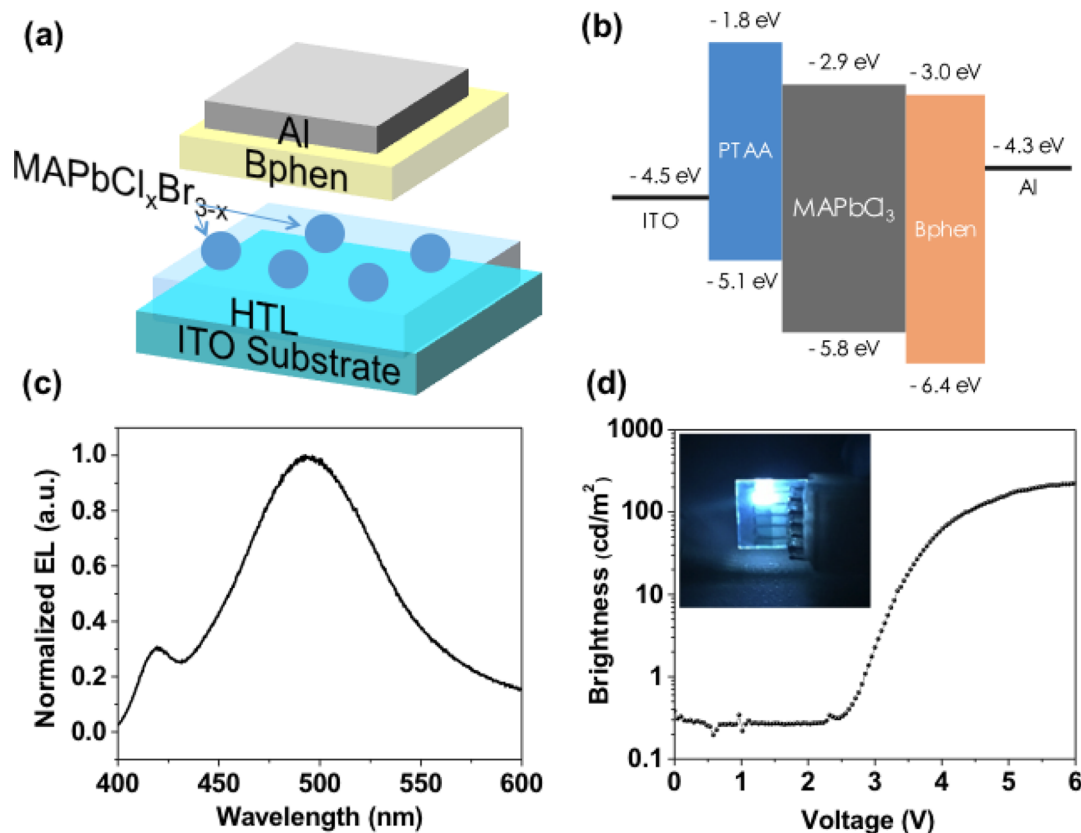


Figure 5. (a) Device structure of the perovskite-based LED. (b) Band diagram of the perovskite based LED. (c) Normalized electroluminescence under a bias of 6 V. (d) Brightness of the device under different bias. Inset is the photo image of the device at 6 V.

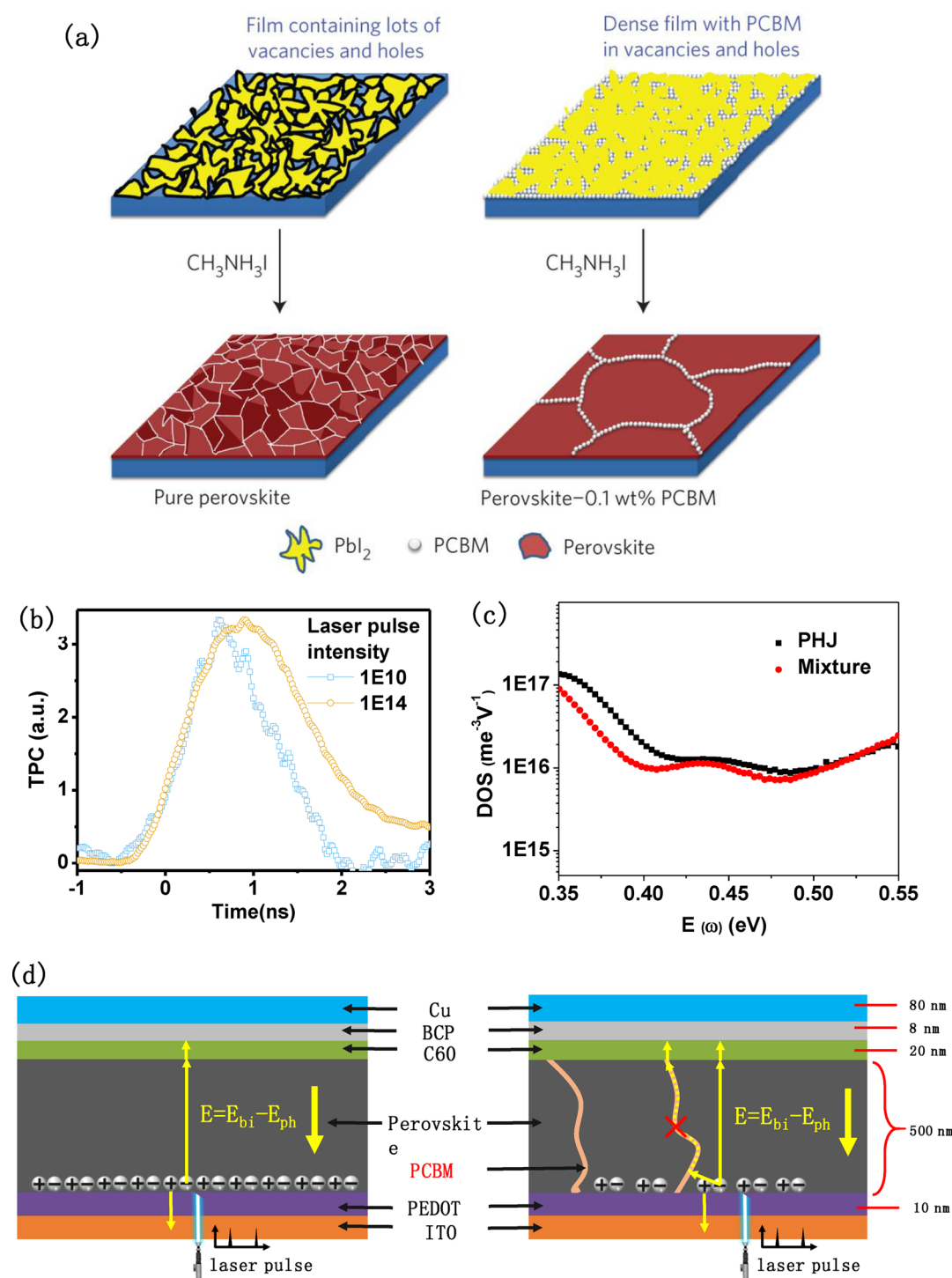
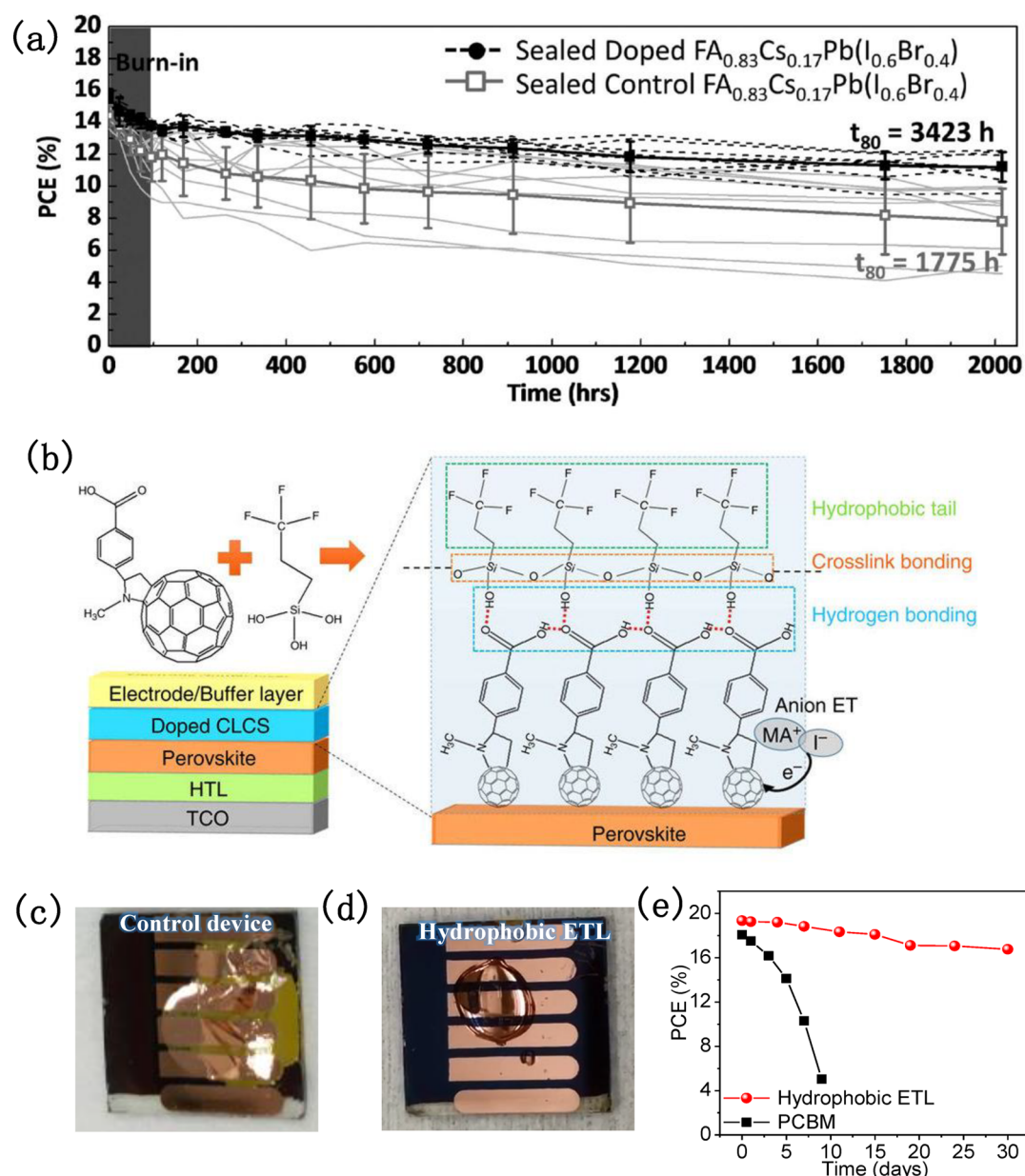


Figure 6. (a) Scheme of the mechanism for the formation of perovskite grains in the absence and presence of PCBM. (Reprinted with permission from ref 32. Copyright 2016 Nature Publishing Group.) (b) Transient photocurrent curves of perovskite photodiode. (Reprinted with permission from ref 42. Copyright 2016 Wiley.) (c) Trap density in fullerene/perovskite PHJ (black curve) and mixture (red curve) devices obtained by TAS measurement. (d) Schematic diagram of the electron transport pathway in fullerene/perovskite PHJ and mixture devices.

PCBM into the grain boundaries (device type II, Figure 6a).<sup>32</sup> An electron transit time of 4.9 ns was recorded, which is limited by the rising time (4 ns) of the pulse laser used here. When we measured the device type I with this pulse laser, we got a similar response time of 4 ns. Such fast response speed is barely possible if electrons go through the fullerene intergranular layer (Figure 6d). A simple calculation indicates that electron transit

time through PCBM intergranular layer across a thickness of 500 nm is around 360–3600 ns with a mobility of  $10^{-3}$ – $10^{-2}$   $\text{cm}^2/(\text{V s})$ . A final question is whether intergranular fullerene will still accept electrons because it does quench photoluminescence of perovskite. We would argue that it is a competition process for electron extraction through perovskite and electron transfer to fullerene. The thickness of the





**Figure 7.** (a) Comparison of stability of FA<sub>0.83</sub>Cs<sub>0.17</sub>Pb(I<sub>0.6</sub>Br<sub>0.4</sub>) perovskite devices with neat (gray curve) and 1 wt % N-DPBI doped C<sub>60</sub> (black curve) electron-transporting layers. The devices were encapsulated and aged under full spectrum simulated AM1.5, 76 mW cm<sup>-2</sup> average irradiance at V<sub>OC</sub> in air without a UV filter. (Reprinted with permission from ref 58. Copyright 2017 Wiley.) (b) Schematic illustration for the cross-linking of C<sub>60</sub>-SAM with silane-coupling agent. Images of the devices based on (c) conventional PCBM and (d) cross-linked C<sub>60</sub>-SAM as ETLs after exposure to water droplet for 4 min. (e) PCE change of the typical perovskite devices with PCBM and cross-linked C<sub>60</sub>-SAM as ETLs stored in an ambient environment without encapsulation. (Reprinted with permission from ref 44. Copyright 2016 Nature Publishing Group.)

intergranular fullerene layer is around 1–3 nm if it is added after perovskite film formation, which is defined by grain boundary geometry.<sup>56</sup> While photogenerated electron affinity to intergranular fullerenes may still transfer to fullerenes, most of the photogenerated electrons would be quickly collected by the built-in field through perovskites with grain size much larger than the electron-transfer distance. In the case in which fullerenes are randomly distributed in perovskite grain boundaries without forming percolation path, the fullerene clusters may still accept some electrons but will act as electron traps.

We thus conclude that the fullerene layer between grain boundaries plays a major role in passivating the defects, which

reduces the charge recombination at grain boundaries and increases the fill factor. It is confirmed by our measurement that the MAPbI<sub>3</sub>:PCBM mixture device had a trap density that was slightly lower than that of the PHJ device (Figure 6c). In this context, other nonconducting materials can replace fullerenes if they can also passivate the defects on the surface of perovskite films and its thickness is small enough so that charge can tunnel through to the electrode. Nevertheless, another important function of the fullerene layer is to separate the perovskite from the electrodes to prevent damage to the perovskite during the deposition of electrodes. Therefore, completely replacing fullerene layers by other functional layers needs to consider all these functions of fullerene layers.

*What Is the Impact of Fullerenes on Device Stability?* To date, there have been barely any stability studies on whether the fullerene layer would limit the stability of perovskite solar cells. Here we discuss the possible influence of fullerenes on perovskite solar cell stability based on the knowledge from organic solar cell studies, which has already reached good conclusions. One big issue with the BHJ structure is that the morphology would change to a thermodynamically more stable state after aging. Under heat, increased diffusivity of fullerenes can increase the domain size of fullerenes and make donor polymers demix from the BHJ, which causes the crystallization of fullerene domains and consequently the loss of device efficiency due to reduction of efficiency in charge generation and extraction. Fortunately, the BHJ structure is not needed in thin-film perovskite solar cells. Thus, the issues with morphology instability of BHJ are not concerns in perovskite solar cells anymore.

Regarding photostability, fullerenes have shown to be able to either stabilize or destabilize the donor polymers from the photooxidation through possible mechanisms of electron extraction, singlet oxygen formation, and radicals.<sup>57</sup> It is still an open question whether the photoinduced polymerization of fullerenes (or dimerization) would cause harmful effect to the perovskite solar cells. Though an initial burn-in was actually observed in the n-i-p structure perovskite solar cells with fullerene as an ultraviolet (UV) filter (Figure 7a),<sup>58</sup> there is no evidence yet this burn-in was caused by the dimerization of fullerene under UV light. Nevertheless, in the p-i-n PHJ solar cells, the perovskite layer works as an optical filter which absorbs most of the higher-energy photons, which should dramatically relieve the pressure on the fullerene layer on photostability. There is increasing interest in applying fullerenes in n-i-p structure solar cells for enhanced efficiency and reduced hysteresis by modifying titanium oxides or tin oxide.<sup>36,38,39,59</sup> In this case, the fullerenes will absorb the high-energy photons, and further study is needed to determine its influence on the oxidation of perovskite as well as their own dimerization.

The leaving of iodine ions from the perovskite layer into the fullerene layer will cause the doping of fullerenes. There is possibility that an enhanced doping of fullerenes may cause the increased e-h recombination at the interface of fullerene and perovskite layers; however, its impact on the charge recombination will depend on the energy structure at the interface that whether there is band-bending at either side of the interface to separate electrons and holes. The band-bending actually occurs in perovskite/single-walled carbon nanotube (SWCNT) interface at the SWCNT side, which results in a very long e-h recombination lifetime of hundreds of microseconds, long enough for the extraction of either type of charge.<sup>19,60</sup> The recombination lifetime at the perovskite/PCBM interface was also shown by us to be close to 1  $\mu$ s for the device even under 1 sun illumination measured with transient photovoltaic technique,<sup>29</sup> which is almost 1000 times longer than the charge transit time across the whole device.<sup>42</sup> Therefore, it seems not an issue to dope fullerene materials for better conductivity.

In terms of moisture stability, the hydrophobic fullerenes may slow the permeation of moisture into the perovskite layer in p-i-n structure devices, but its structure may be still too loose to prevent moisture permeation. To enhance the water resistance of the fullerene layer, Bai et al. introduced cross-linkable silane molecules with hydroxyl groups to be bonded onto carboxyl group ( $-\text{COOH}$ ) of a fullerene derivative, and

the hydrophobic functional  $-\text{CF}_3$  groups of the bonding molecules effectively prevent the permeation of water, as demonstrated by water stability measurements (Figure 7b–d).<sup>44</sup> The devices showed a high PCE of 19.5% and maintained 90% of their original PCE after storage in air for 30 days.<sup>44</sup> One interesting phenomenon is that the cross-linking of the silane layer also aligned the fullerene layer, which reduced energy disorder and retained the large  $V_{\text{OC}}$ . The silane layer has to be thin so that electrons can tunnel through, which somehow limits the water resistivity of this layer.

*Summary and Future Outlook.* There has been tremendous progress in applying fullerene to improve the performance of perovskite solar cells. In comparison to the commonly used inorganic ETL,  $\text{TiO}_2$ , fullerene can be deposited by a low-temperature solution method and shows much better performance in elimination of current hysteresis of perovskite solar cells. This is largely caused by the trap passivation and ion-migration blocking functions of fullerene on perovskite surface and in grain boundaries and fast charge transfer between the fullerene and perovskite. We also discussed the working mechanism of perovskite/fullerene blend film-based solar cells and pointed out that it is unlikely to work as a BHJ solar cell because of the electron mobility of most perovskites is much larger than that of fullerenes. In terms of  $V_{\text{OC}}$  output, we demonstrated that fullerene-based perovskite solar cells do not necessarily possess lower  $V_{\text{OC}}$  in comparison to that of  $\text{TiO}_2$ -based solar cells, as long as the energy disorder is mitigated. In future studies, the conductivity of the fullerene layer needs to be further increased so that it can be thick enough to encapsulate the perovskite layer while still maintaining the low series resistance of the device. Also, it is desirable to find environmentally benign solvents to replace the toxic chlorobenzene or dichlorobenzene for the processing of soluble fullerenes. Finally, there is still much work remaining to be done to fully understand whether the intrinsic stability of fullerene would limit the stability of perovskite solar cells, which is the key to the practical application of perovskite solar cells.

## ■ METHOD

*Fabrication of Perovskite-Based LED.* The ITO substrate was cleaned in  $\text{O}_3$  plasma, and a thin layer of PTAA (0.2 wt % dissolved in 1,2-dichlorobenzene) was spin-coated on it at 6000 rpm. The perovskite layer was deposited on PTAA by a two-step process:  $\text{PbBr}_2$  (50 mg/mL dissolved in N,N-dimethylformamide, DMF) was spin-coated at 6000 rpm and annealed on the hot plate at 100 °C for 10 min. Then, MAI (15 mg/mL dissolved in ethanol) was spin-coated on the  $\text{PbBr}_2$  layer and annealed on the hot plate at 100 °C for 30 min. The Bphen layer and Al electrode were thermally evaporated sequentially, with thicknesses of 30 and 80 nm, respectively.

*Fabrication of PHJ-PSC and Mixture-PSC.* The PHJ-PSC device was fabricated following the typical procedure of interdiffusion method. The PEDOT:PSS layer was spin-coated on  $\text{O}_3$  plasma-treated ITO substrates at 4000 rpm. After being annealed at 140 °C for 20 min in air, the substrates were transferred to a  $\text{N}_2$  glovebox where 630 mg/mL  $\text{PbI}_2$  solution (DMF as solvent) and 65 mg/mL MAI solution (IPA as solvent) were spin coated sequentially. Then the substrates were annealed at 100 °C for 60 min to form uniform perovskite films.  $\text{C}_{60}$ , BCP, and Cu layers were thermally evaporated onto perovskite in sequence.

The fabrication procedure of mixture-PSC device was the same as that of PHJ–PSCs except 0.1 wt % PCBM was premixed in the  $\text{PbI}_2$  solution.

**Characterization.** The thermal admittance spectroscopy was performed by an Agilent E4980A Precision LCR meter. The trap densities in PHJ–PSC and mixture-PSC are derived from the following equations:

$$E_{\omega} = k_{\text{B}}T \ln\left(\frac{\omega_0}{\omega}\right)$$

$$N_{\text{T}}(E_{\omega}) = -\frac{V_{\text{bi}}}{qW} \frac{dC}{d\omega} \frac{\omega}{k_{\text{B}}T}$$

where  $C$  is the capacitance,  $\omega$  the angular frequency,  $q$  the elementary charge,  $k_{\text{B}}$  Boltzmann's constant, and  $T$  the temperature.  $V_{\text{bi}}$  and  $W$  are the built-in potential and depletion width, respectively, and  $\omega_0$  is the attempt-to-escape frequency.

## AUTHOR INFORMATION

### Corresponding Author

\*E-mail: [jhuang2@unl.edu](mailto:jhuang2@unl.edu).

### ORCID

Jinsong Huang: [0000-0002-0509-8778](https://orcid.org/0000-0002-0509-8778)

### Notes

The authors declare no competing financial interest.

### Biographies

**Dr. Yanjun Fang** received his B.S. and Ph.D. degrees from Department of Physics, Zhejiang University. He is currently a postdoctoral researcher at Department of Mechanical & Materials Engineering, University of Nebraska—Lincoln. His research interests include the device physics of perovskite solar cells and photodetectors.

**Mr. Cheng Bi** received his B.S. and M.S. degrees in Material Science and Engineering from Donghua University. He is currently a Ph.D. student at University of Nebraska—Lincoln. His research focuses on perovskite solar cells and light-emitting diodes.

**Mr. Dong Wang** received his M.S. degree from Qingdao Institute of Bioenergy and Bioprocess Technology, Chinese Academy of Sciences. Thereafter, he joined Prof. Huang's group as a Ph.D. student. His research interests include engineering and physics of perovskite solar cells.

**Prof. Jinsong Huang** received his Ph.D. degree in Material Science and Engineering from the University of California—Los Angeles in 2007. He is now the Susan J. Rosowski Professor in the Department of Mechanical Engineering at University of Nebraska—Lincoln (UNL). His current research interests include solution-processed electronic materials for applications in sensing, energy, and consumer electronics. More information can be found at [www.huanggroup.unl.edu](http://www.huanggroup.unl.edu).

## ACKNOWLEDGMENTS

This work was supported in part by Air Force Office of Scientific Research (AFOSR) (Grant No. A9550-16-1-0299) and the National Science Foundation (NSF) Grant OIA-1538893.

## REFERENCES

(1) Stranks, S. D.; Eperon, G. E.; Grancini, G.; Menelaou, C.; Alcocer, M. J. P.; Leijtens, T.; Herz, L. M.; Petrozza, A.; Snaith, H. J. Electron-Hole Diffusion Lengths Exceeding 1 Micrometer in an Organometal Trihalide Perovskite Absorber. *Science* **2013**, *342*, 341–344.

(2) Xing, G.; Mathews, N.; Sun, S.; Lim, S. S.; Lam, Y. M.; Grätzel, M.; Mhaisalkar, S.; Sum, T. C. Long-Range Balanced Electron- and Hole-Transport Lengths in Organic-Inorganic  $\text{CH}_3\text{NH}_3\text{PbI}_3$ . *Science* **2013**, *342*, 344–347.

(3) Dong, Q.; Fang, Y.; Shao, Y.; Mulligan, P.; Qiu, J.; Cao, L.; Huang, J. Electron-Hole Diffusion Lengths > 175 nm in Solution-Grown  $\text{CH}_3\text{NH}_3\text{PbI}_3$  Single Crystals. *Science* **2015**, *347*, 967–970.

(4) Shi, D.; Adinolfi, V.; Comin, R.; Yuan, M.; Alarousu, E.; Buin, A.; Chen, Y.; Hoogland, S.; Rothenberger, A.; Katsiev, K.; et al. Low Trap-State Density and Long Carrier Diffusion in Organolead Trihalide Perovskite Single Crystals. *Science* **2015**, *347*, 519–522.

(5) Stoumpos, C. C.; Malliakas, C. D.; Kanatzidis, M. G. Semiconducting Tin and Lead Iodide Perovskites with Organic Cations: Phase Transitions, High Mobilities, and Near-Infrared Photoluminescent Properties. *Inorg. Chem.* **2013**, *52*, 9019–9038.

(6) Green, M. A.; Ho-Baillie, A.; Snaith, H. J. The Emergence of Perovskite Solar Cells. *Nat. Photonics* **2014**, *8*, 506–514.

(7) Yang, W. S.; Noh, J. H.; Jeon, N. J.; Kim, Y. C.; Ryu, S.; Seo, J.; Seok, S. I. High-Performance Photovoltaic Perovskite Layers Fabricated through Intramolecular Exchange. *Science* **2015**, *348*, 1234–1237.

(8) Best Research-Cell Efficiency. <http://www.nrel.gov/pv/assets/images/efficiency-chart.png> (accessed 2016).

(9) Bi, D.; Tress, W.; Dar, M. I.; Gao, P.; Luo, J.; Renevier, C.; Schenk, K.; Abate, A.; Giordano, F.; Correa Baena, J.-P.; et al. Efficient Luminescent Solar Cells Based on Tailored Mixed-Cation Perovskites. *Sci. Adv.* **2016**, *2*, e1501170.

(10) Li, X.; Bi, D.; Yi, C.; Décoppet, J.-D.; Luo, J.; Zakeeruddin, S. M.; Hagfeldt, A.; Grätzel, M. A Vacuum Flash-Assisted Solution Process for High-Efficiency Large-Area Perovskite Solar Cells. *Science* **2016**, *353*, 58–62.

(11) Bi, D.; Yi, C.; Luo, J.; Décoppet, J.-D.; Zhang, F.; Zakeeruddin, S. M.; Li, X.; Hagfeldt, A.; Grätzel, M. Polymer-Templated Nucleation and Crystal Growth of Perovskite Films for Solar Cells with Efficiency Greater Than 21%. *Nat. Energy* **2016**, *1*, 16142.

(12) Wang, Q.; Dong, Q.; Li, T.; Gruverman, A.; Huang, J. Thin Insulating Tunneling Contacts for Efficient and Water-Resistant Perovskite Solar Cells. *Adv. Mater.* **2016**, *28*, 6734–6739.

(13) Saliba, M.; Matsui, T.; Seo, J.-Y.; Domanski, K.; Correa-Baena, J.-P.; Nazeeruddin, M. K.; Zakeeruddin, S. M.; Tress, W.; Abate, A.; Hagfeldt, A.; et al. Cesium-Containing Triple Cation Perovskite Solar Cells: Improved Stability, Reproducibility and High Efficiency. *Energy Environ. Sci.* **2016**, *9*, 1989–1997.

(14) Mei, A.; Li, X.; Liu, L.; Ku, Z.; Liu, T.; Rong, Y.; Xu, M.; Hu, M.; Chen, J.; Yang, Y.; et al. A Hole-Conductor-Free, Fully Printable Mesoscopic Perovskite Solar Cell with High Stability. *Science* **2014**, *345*, 295–298.

(15) Chen, H.; Pan, X.; Liu, W.; Cai, M.; Kou, D.; Huo, Z.; Fang, X.; Dai, S. Efficient Panchromatic Inorganic-Organic Heterojunction Solar Cells with Consecutive Charge Transport Tunnels in Hole Transport Material. *Chem. Commun.* **2013**, *49*, 7277–7279.

(16) Habisreutinger, S. N.; Leijtens, T.; Eperon, G. E.; Stranks, S. D.; Nicholas, R. J.; Snaith, H. J. Carbon Nanotube/Polymer Composites as a Highly Stable Hole Collection Layer in Perovskite Solar Cells. *Nano Lett.* **2014**, *14*, 5561–5568.

(17) Habisreutinger, S. N.; Leijtens, T.; Eperon, G. E.; Stranks, S. D.; Nicholas, R. J.; Snaith, H. J. Enhanced Hole Extraction in Perovskite Solar Cells through Carbon Nanotubes. *J. Phys. Chem. Lett.* **2014**, *5*, 4207–4212.

(18) Li, Z.; Kulkarni, S. A.; Boix, P. P.; Shi, E.; Cao, A.; Fu, K.; Batabyal, S. K.; Zhang, J.; Xiong, Q.; Wong, L. H.; et al. Laminated Carbon Nanotube Networks for Metal Electrode-Free Efficient Perovskite Solar Cells. *ACS Nano* **2014**, *8*, 6797–6804.

(19) Ihly, R.; Dowgiallo, A.-M.; Yang, M.; Schulz, P.; Stanton, N. J.; Reid, O. G.; Ferguson, A. J.; Zhu, K.; Berry, J. J.; Blackburn, J. L. Efficient Charge Extraction and Slow Recombination in Organic-Inorganic Perovskites Capped with Semiconducting Single-Walled Carbon Nanotubes. *Energy Environ. Sci.* **2016**, *9*, 1439–1449.

- (20) Wang, J. T.-W.; Ball, J. M.; Barea, E. M.; Abate, A.; Alexander-Webber, J. A.; Huang, J.; Saliba, M.; Mora-Sero, L.; Bisquert, J.; Snaith, H. J.; et al. Low-Temperature Processed Electron Collection Layers of Graphene/TiO<sub>2</sub> Nanocomposites in Thin Film Perovskite Solar Cells. *Nano Lett.* **2014**, *14*, 724–730.
- (21) Yoon, J.; Sung, H.; Lee, G.; Cho, W.; Ahn, N.; Jung, H. S.; Choi, M. Superflexible, High-Efficiency Perovskite Solar Cells Utilizing Graphene Electrodes: Towards Future Foldable Power Sources. *Energy Environ. Sci.* **2017**, *10*, 337.
- (22) Hadadian, M.; Correa-Baena, J.-P.; Goharshadi, E. K.; Ummadisingu, A.; Seo, J.-Y.; Luo, J.; Gholipour, S.; Zakeeruddin, S. M.; Saliba, M.; Abate, A.; et al. Enhancing Efficiency of Perovskite Solar Cells Via N-Doped Graphene: Crystal Modification and Surface Passivation. *Adv. Mater.* **2016**, *28*, 8681–8686.
- (23) Jeng, J.-Y.; Chiang, Y.-F.; Lee, M.-H.; Peng, S.-R.; Guo, T.-F.; Chen, P.; Wen, T.-C. CH<sub>3</sub>NH<sub>3</sub>PbI<sub>3</sub> Perovskite/Fullerene Planar-Heterojunction Hybrid Solar Cells. *Adv. Mater.* **2013**, *25*, 3727–3732.
- (24) Sun, S.; Salim, T.; Mathews, N.; Duchamp, M.; Boothroyd, C.; Xing, G.; Sum, T. C.; Lam, Y. M. The Origin of High Efficiency in Low-Temperature Solution-Processable Bilayer Organometal Halide Hybrid Solar Cells. *Energy Environ. Sci.* **2014**, *7*, 399–407.
- (25) Wang, Q.; Shao, Y.; Dong, Q.; Xiao, Z.; Yuan, Y.; Huang, J. Large Fill-Factor Bilayer Iodine Perovskite Solar Cells Fabricated by a Low-Temperature Solution-Process. *Energy Environ. Sci.* **2014**, *7*, 2359–2365.
- (26) Xiao, Z.; Bi, C.; Shao, Y.; Dong, Q.; Wang, Q.; Yuan, Y.; Wang, C.; Gao, Y.; Huang, J. Efficient, High Yield Perovskite Photovoltaic Devices Grown by Interdiffusion of Solution-Processed Precursor Stacking Layers. *Energy Environ. Sci.* **2014**, *7*, 2619–2623.
- (27) Bi, C.; Wang, Q.; Shao, Y.; Yuan, Y.; Xiao, Z.; Huang, J. Non-Wetting Surface-Driven High-Aspect-Ratio Crystalline Grain Growth for Efficient Hybrid Perovskite Solar Cells. *Nat. Commun.* **2015**, *6*, 7747.
- (28) Dong, Q.; Yuan, Y.; Shao, Y.; Fang, Y.; Wang, Q.; Huang, J. Abnormal Crystal Growth in CH<sub>3</sub>NH<sub>3</sub>PbI<sub>3-x</sub>Cl<sub>x</sub> Using a Multi-Cycle Solution Coating Process. *Energy Environ. Sci.* **2015**, *8*, 2464–2470.
- (29) Shao, Y.; Yuan, Y.; Huang, J. Correlation of Energy Disorder and Open-Circuit Voltage in Hybrid Perovskite Solar Cells. *Nat. Energy* **2016**, *1*, 15001.
- (30) Shao, Y.; Xiao, Z.; Bi, C.; Yuan, Y.; Huang, J. Origin and Elimination of Photocurrent Hysteresis by Fullerene Passivation in CH<sub>3</sub>NH<sub>3</sub>PbI<sub>3</sub> Planar Heterojunction Solar Cells. *Nat. Commun.* **2014**, *5*, 5784.
- (31) Xu, J.; Buin, A.; Ip, A. H.; Li, W.; Voznyy, O.; Comin, R.; Yuan, M.; Jeon, S.; Ning, Z.; McDowell, J. J.; et al. Perovskite–Fullerene Hybrid Materials Suppress Hysteresis in Planar Diodes. *Nat. Commun.* **2015**, *6*, 7081.
- (32) Chiang, C.-H.; Wu, C.-G. Bulk Heterojunction Perovskite–PCBM Solar Cells with High Fill Factor. *Nat. Photonics* **2016**, *10*, 196–200.
- (33) Wang, K.; Liu, C.; Du, P.; Zheng, J.; Gong, X. Bulk Heterojunction Perovskite Hybrid Solar Cells with Large Fill Factor. *Energy Environ. Sci.* **2015**, *8*, 1245–1255.
- (34) Wu, Y.; Yang, X.; Chen, W.; Yue, Y.; Cai, M.; Xie, F.; Bi, E.; Islam, A.; Han, L. Perovskite Solar Cells with 18.21% Efficiency and Area over 1 cm<sup>2</sup> Fabricated by Heterojunction engineering. *Nat. Energy* **2016**, *1*, 16148.
- (35) Abrusci, A.; Stranks, S. D.; Docampo, P.; Yip, H.-L.; Jen, A. K. Y.; Snaith, H. J. High-Performance Perovskite-Polymer Hybrid Solar Cells Via Electronic Coupling with Fullerene Monolayers. *Nano Lett.* **2013**, *13*, 3124–3128.
- (36) Wojciechowski, K.; Stranks, S. D.; Abate, A.; Sadoughi, G.; Sadhanala, A.; Kopydakis, N.; Rumbles, G.; Li, C.-Z.; Friend, R. H.; Jen, A. K. Y.; et al. Heterojunction Modification for Highly Efficient Organic–Inorganic Perovskite Solar Cells. *ACS Nano* **2014**, *8*, 12701–12709.
- (37) Tao, C.; Neutzner, S.; Colella, L.; Marras, S.; Srimath Kandada, A. R.; Gandini, M.; Bastiani, M. D.; Pace, G.; Manna, L.; Caironi, M.; et al. 17.6% Stabilized Efficiency in Low-Temperature Processed Planar Perovskite Solar Cells. *Energy Environ. Sci.* **2015**, *8*, 2365–2370.
- (38) Zhong, Y.; Munir, R.; Balawi, A. H.; Sheikh, A. D.; Yu, L.; Tang, M.-C.; Hu, H.; Laquai, F.; Amassian, A. Mesostructured Fullerene Electrodes for Highly Efficient n–i–p Perovskite Solar Cells. *ACS Energy Lett.* **2016**, *1*, 1049–1056.
- (39) Li, Y.; Zhao, Y.; Chen, Q.; Yang, Y.; Liu, Y.; Hong, Z.; Liu, Z.; Hsieh, Y.-T.; Meng, L.; Li, Y.; et al. Multifunctional Fullerene Derivative for Interface Engineering in Perovskite Solar Cells. *J. Am. Chem. Soc.* **2015**, *137*, 15540–15547.
- (40) Snaith, H. J.; Abate, A.; Ball, J. M.; Eperon, G. E.; Leijtens, T.; Noel, N. K.; Stranks, S. D.; Wang, J. T.-W.; Wojciechowski, K.; Zhang, W. Anomalous Hysteresis in Perovskite Solar Cells. *J. Phys. Chem. Lett.* **2014**, *5*, 1511–1515.
- (41) Shao, Y.; Fang, Y.; Li, T.; Wang, Q.; Dong, Q.; Deng, Y.; Yuan, Y.; Wei, H.; Wang, M.; Gruverman, A.; et al. Grain Boundary Dominated Ion Migration in Polycrystalline Organic-Inorganic Halide Perovskite Films. *Energy Environ. Sci.* **2016**, *9*, 1752–1759.
- (42) Shen, L.; Fang, Y.; Wang, D.; Bai, Y.; Deng, Y.; Wang, M.; Lu, Y.; Huang, J. A Self-Powered, Sub-Nanosecond-Response Solution-Processed Hybrid Perovskite Photodetector for Time-Resolved Photoluminescence-Lifetime Detection. *Adv. Mater.* **2016**, *28*, 10794–10800.
- (43) Fang, Y.; Huang, J. Resolving Weak Light of Sub-Picowatt Per Square Centimeter by Hybrid Perovskite Photodetectors Enabled by Noise Reduction. *Adv. Mater.* **2015**, *27*, 2804–2810.
- (44) Bai, Y.; Dong, Q.; Shao, Y.; Deng, Y.; Wang, Q.; Shen, L.; Wang, D.; Wei, W.; Huang, J. Enhancing Stability and Efficiency of Perovskite Solar Cells with Crosslinkable Silane-Functionalized and Doped Fullerene. *Nat. Commun.* **2016**, *7*, 12806.
- (45) Li, C.-Z.; Chueh, C.-C.; Ding, F.; Yip, H.-L.; Liang, P.-W.; Li, X.; Jen, A. K. Y. Doping of Fullerenes Via Anion-Induced Electron Transfer and Its Implication for Surfactant Facilitated High Performance Polymer Solar Cells. *Adv. Mater.* **2013**, *25*, 4425–4430.
- (46) Bryant, D.; Wheeler, S.; O'Regan, B. C.; Watson, T.; Barnes, P. R. F.; Worsley, D.; Durrant, J. Observable Hysteresis at Low Temperature in “Hysteresis Free” Organic–Inorganic Lead Halide Perovskite Solar Cells. *J. Phys. Chem. Lett.* **2015**, *6*, 3190–3194.
- (47) Wu, K.; Bera, A.; Ma, C.; Du, Y.; Yang, Y.; Li, L.; Wu, T. Temperature-Dependent Excitonic Photoluminescence of Hybrid Organometal Halide Perovskite Films. *Phys. Chem. Chem. Phys.* **2014**, *16*, 22476–22481.
- (48) D’Innocenzo, V.; Grancini, G.; Alcocer, M. J. P.; Kandada, A. R. S.; Stranks, S. D.; Lee, M. M.; Lanzani, G.; Snaith, H. J.; Petrozza, A. Excitons Versus Free Charges in Organo-Lead Tri-Halide Perovskites. *Nat. Commun.* **2014**, *5*, 3586.
- (49) He, H.; Yu, Q.; Li, H.; Li, J.; Si, J.; Jin, Y.; Wang, N.; Wang, J.; He, J.; Wang, X.; et al. Exciton Localization in Solution-Processed Organolead Trihalide Perovskites. *Nat. Commun.* **2016**, *7*, 10896.
- (50) Hu, M.; Bi, C.; Yuan, Y.; Xiao, Z.; Dong, Q.; Shao, Y.; Huang, J. Distinct Exciton Dissociation Behavior of Organolead Trihalide Perovskite and Excitonic Semiconductors Studied in the Same System. *Small* **2015**, *11*, 2164–2169.
- (51) Seo, J.; Park, S.; Chan Kim, Y.; Jeon, N. J.; Noh, J. H.; Yoon, S. C.; Seok, S. I. Benefits of Very Thin PCBM and LiF Layers for Solution-Processed p-i-n Perovskite Solar Cells. *Energy Environ. Sci.* **2014**, *7*, 2642–2646.
- (52) You, J.; Hong, Z.; Yang, Y.; Chen, Q.; Cai, M.; Song, T.-B.; Chen, C.-C.; Lu, S.; Liu, Y.; Zhou, H.; et al. Low-Temperature Solution-Processed Perovskite Solar Cells with High Efficiency and Flexibility. *ACS Nano* **2014**, *8*, 1674–1680.
- (53) Malinkiewicz, O.; Yella, A.; Lee, Y. H.; Espallargas, G. M.; Graetzel, M.; Nazeeruddin, M. K.; Bolink, H. J. Perovskite Solar Cells Employing Organic Charge-Transport Layers. *Nat. Photonics* **2014**, *8*, 128–132.
- (54) Tummala, N. R.; Zheng, Z.; Aziz, S. G.; Coropceanu, V.; Brédas, J.-L. Static and Dynamic Energetic Disorders in the C60, PC61BM, C70, and PC71BM Fullerenes. *J. Phys. Chem. Lett.* **2015**, *6*, 3657–3662.

(55) Bai, Y.; Fang, Y.; Deng, Y.; Wang, Q.; Zhao, J.; Zheng, X.; Zhang, Y.; Huang, J. Low Temperature Solution-Processed Sb:SnO<sub>2</sub> Nanocrystals for Efficient Planar Perovskite Solar Cells. *ChemSusChem* **2016**, *9*, 2686–2691.

(56) Wang, Q.; Chen, B.; Liu, Y.; Deng, Y.; Bai, Y.; Dong, Q.; Huang, J. Scaling Behavior of Moisture-Induced Grain Degradation in Polycrystalline Hybrid Perovskite Thin Films. *Energy Environ. Sci.* **2016**, *10*, 516.

(57) Fraga Domínguez, I.; Distler, A.; Lüer, L. Stability of Organic Solar Cells: The Influence of Nanostructured Carbon Materials. *Adv. Energy Mater.* **2016**, 1601320.

(58) Wang, Z.; McMeekin, D. P.; Sakai, N.; van Reenen, S.; Wojciechowski, K.; Patel, J. B.; Johnston, M. B.; Snaith, H. J. Efficient and Air-Stable Mixed-Cation Lead Mixed-Halide Perovskite Solar Cells with n-Doped Organic Electron Extraction Layers. *Adv. Mater.* **2017**, *29*, 1604186.

(59) Ke, W.; Zhao, D.; Xiao, C.; Wang, C.; Cimaroli, A. J.; Grice, C. R.; Yang, M.; Li, Z.; Jiang, C.-S.; Al-Jassim, M.; et al. Cooperative Tin Oxide Fullerene Electron Selective Layers for High-Performance Planar Perovskite Solar Cells. *J. Mater. Chem. A* **2016**, *4*, 14276–14283.

(60) Schulz, P.; Dowgiallo, A.-M.; Yang, M.; Zhu, K.; Blackburn, J. L.; Berry, J. J. Charge Transfer Dynamics between Carbon Nanotubes and Hybrid Organic Metal Halide Perovskite Films. *J. Phys. Chem. Lett.* **2016**, *7*, 418–425.